Effective microscopic model for the dynamics of spreading

J. De Coninck,[1] S. Hoorelbeke,[1] M. P. Valignat,[2] and A. M. Cazabat[2]
[1]*Faculté des Sciences, Université de Mons-Hainaut, Place du Parc, 20, 7000 Mons, Belgium*
[2]*Laboratoire de Physique de la Matière Condensée, 11, Collège de France, Place Marcelin-Berthelot, 75231 Paris Cedex 05, France*
(Received 22 July 1993)

An effective microscopic model for the dynamics of spreading is considered within the class of solid-on-solid models. The dynamics is of Kawasaki type, which implies local conservation of matter. Experimental results are presented and compared with microscopic simulations. The general agreement between the observations and this microscopic model is very satisfactory.

PACS number(s): 68.10.−m, 68.45.Gd, 05.50.+q

I. INTRODUCTION

The dynamics of spreading of a drop on top of a wall has been a very active field of research during the last years. Many recent experiments at the microscopic level have revealed new phenomena as the appearance of a monolayer in front of the drop [1,2], two diffusive regimes for the radius of the drop as a function of the time [3], stratified profiles [4], etc.

Several microscopic models have been considered within the literature based on molecular [5,6] or Kawasaki dynamics for a lattice gas [3]. Up to now, it seems that the molecular-dynamical model, for which the equations of motion are solved at each step for each particle, developed by Koplik and co-workers [5] and Abraham and co-workers [6] does not lead to the recovery of the main experimental observations possibly because of the huge disproportion between the longitudinal scales involved: in the model, thickness and longitudinal scales are microscopic while in the experiment the longitudinal scale is macroscopic. Kawasaki dynamics recovers the experimental results but the great number of molecules required for the numerical simulations does not allow a more detailed study of the different parameters which appear within the problem.

It is therefore of interest to consider an effective model providing a clear interpretation of the experimental observations in terms of microscopic considerations.

To reduce the greater number of degrees of freedom of the problem, we consider an effective model of the interface in terms of a solid-on-solid (SOS) approximation. A few steps have already been performed in this direction but without recovering the experimental observations: SOS models and Langevin dynamics [7], SOS models and Monte Carlo dynamics [8], etc. It is our aim here to develop an approach of the SOS models using Monte Carlo dynamics by imposing the local conservation of material. In other words, we study here the Kawasaki dynamics within SOS models.

Another advantage of the SOS model is that it allows to study nonvolatile liquid drops: this model is thus closer to the actual experiments than the "bulk models."

Experiments deal with microdroplets of nonvolatile liquids spreading spontaneously on smooth solid surfaces. The liquids are nonvolatile at three dimensions, i.e., the volume of the drops does not change with time, but also at two dimensions. In these conditions, the drops take a striking step-pyramidal shape [4], the height of each step being the molecule size. The requirement of nonvolatility at two dimensions ensures that the step edge is not smoothed out by thermal motion. The droplet shape, i.e., the relative length of the successive steps, is largely controlled by the behavior of the first monolayer. If this layer develops rapidly, because of favorable energy balance or especially low friction, the next layers will not grow: all the drop will be emptied through the first layer. In the opposite case, all the layers grow more or less at the same rate, and up to seven steps are visible on the drop profile [9].

The experimental setup is a modulated ellipsometer with high lateral (30 μm) and thickness (0.2 Å) resolution, which has been described elsewhere [1,2]. The liquids are light nonvolatile polydimethylsiloxanes (PDMS). Although these molecules are (short) polymers, they mostly behave like simple liquids in our investigations [2,4,9]. The successive steps are formed of molecules in a flat configuration, the thickness of the steps being the transverse size of the monomer. No polymeric effects as entanglements occur in our range of molecular weights. The substrates are oxidized silicon wafers, which provide smooth high-energy surfaces. In some cases, a low-energy layer is grafted or deposited on the surface. Until recently, we used layers which were less wettable than the bare wafer, but still wettable by PDMS. This means that the interaction between PDMS molecules and substrate has a monotonous dependence in film thickness (i.e., in distance to the substrate).

More recently, we have been interested in situations where the thickness dependence of the interaction between liquid molecules and solid surface is not monotonous: the long-range part of the interaction favors wetting, while the short-range part opposes it. This is achieved by grafting layers which are not wettable by PDMS, while the bare substrate is wettable. If the grafted layer is thick enough, or if its surface energy is very low, the PDMS will not wet the grafted surface. A tran-

sition takes place between a wetting situation (the bare substrate wins) and a nonwetting one (the grafted layer dominates). New features appear in the drop profile close to the wetting transition: the first step becomes thicker than the molecule size, and its thickness increases when the transition is approached [10].

II. THE MODEL

Let us consider a drop of a liquid B in equilibrium with a phase A on top of a substrate (wall: W). The corresponding A/B interface may be described by a collection of integers $h_0, h_1, \ldots, h_L \geq 0$, assuming no overhangs (this is what is called a "SOS approximation"). A typical configuration is given in Fig. 1.

The energetic cost of this interface is given by

$$\begin{aligned} H(h_0,\ldots,h_L) &= J_{AB}\sum_{i=0}^{L-1}|h_{i+1}-h_i| + J_{AB}\sum_{i=0}^{L}(1-\delta_{h_i,0}) \\ &\quad + J_{BW}\sum_{i=0}^{L}(1-\delta_{h_i,0}) + J_{AW}\sum_{i=0}^{L}\delta_{h_i,0}\ , \\ H(h_0,\ldots,h_L) &= J_{AB}\sum_{i=0}^{L-1}|h_{i+1}-h_i| \\ &\quad + (J_{AW}-J_{BW}-J_{AB})\sum_{i=0}^{L}\delta_{h_i,0} \\ &\quad + (J_{AB}+J_{BW})L\ , \end{aligned} \tag{1}$$

where the different energetic constants J_{AB}, J_{AW}, J_{BW} have been introduced in Fig. 1. The associated free energies γ_{AB} and $\gamma_{AW}-\gamma_{BW}$ are orientational dependent due to the lattice approximation and are given by (more details are presented in the Appendix)

$$\gamma_{AB}(\theta=0) = -\frac{1}{\beta}\lim_{L\to\infty}\frac{1}{L}\ln\left[\sum_{h_0=0,\,h_1\in\mathbb{Z}}\cdots\sum_{h_{L-1}\in\mathbb{Z},h_L=0}\exp\left[-\beta J_{AB}\sum_{i=0}^{L-1}[1+|h_{i+1}-h_i|]\right]\right] \tag{2}$$

and

$$\begin{aligned} \gamma_{AW}-\gamma_{BW} = -\frac{1}{\beta}\lim_{L\to\infty}\frac{1}{L}\ln\Bigg[&\sum_{h_0\in\mathbb{Z}^+}\cdots\sum_{h_L\in\mathbb{Z}^+}\exp\left\{-\beta\left[J_{AB}\sum_{i=0}^{L-1}|h_{i+1}-h_i|\right]\right\} \\ &\times\exp\left[\left\{-\beta\left[(J_{AW}-J_{BW}-J_{AB})\sum_{i=0}^{L}\delta_{h_i,0}+J_{AB}L\right]\right\}\right]\Bigg]\ . \end{aligned} \tag{3}$$

We then let evolve the system according to a Monte Carlo dynamics which preserves locally the volume of the drop. At each step, we thus consider the possible changes for $i=0,1,2,\ldots,L-1$:

$$(h_i,h_{i+1})\to\begin{cases}(h_i',h_{i+1}')=(h_i+1,h_{i+1}-1)\\(h_i',h_{i+1}')=(h_i,h_{i+1})\\(h_i',h_{i+1}')=(h_i-1,h_{i+1}+1)\ .\end{cases} \tag{4}$$

The transition probability is defined using the Boltzmann factor corresponding to the Hamiltonian (1)

$$p=\frac{1}{1+e^{\Delta H/kT}}\ , \tag{5}$$

where k is the Boltzmann constant, T is the temperature

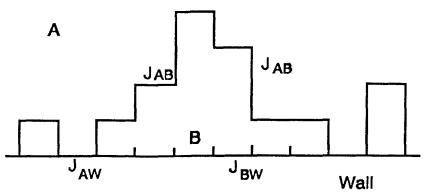

FIG. 1. A typical configuration showing the costs in energy: J_{AB} for a horizontal or vertical portion of the A/B interface; J_{AW} and J_{BW}, respectively, for the contact of A and B with the wall.

and

$$\Delta H = H(h_i',h_{i+1}')-H(h_i,h_{i+1})\ . \tag{6}$$

III. THE DYNAMICS

The choice of the dynamics remains on the Kawasaki model and its convergence to equilibrium is discussed in the Appendix.

As already pointed out in the presentation of the model, we have considered the Monte Carlo dynamics with a local conservation of the volume applied to the shape of a SOS drop. For a complete wetting regime, given by

$$\gamma_{AW}-\gamma_{BW}\geq\gamma_{AB}(\theta=0)\ , \tag{7}$$

where $\gamma_{AW}-\gamma_{BW}$ represents the difference of wall free energies and $\gamma_{AB}(\theta=0)$ is the interfacial tension for a flat interface ($\theta=0$); we may thus study the time behavior of the radius of the drop for different values of $\gamma_{AB}(\theta=0)$ and different types of wall attractions contained in $\gamma_{AW}-\gamma_{BW}$. The general class of models we will consider is given by the following Hamiltonian:

$$\begin{aligned} H(h_0,\ldots,h_L) &= J_{AB}\sum_i(|h_{i+1}-h_i|+1) \\ &\quad + J_{BW}L+\sum_i\mu(h_i) \end{aligned} \tag{8}$$

with

$$\mu(0)=J_{AW}-J_{BW}-J_{AB} ,$$
$$\mu(h_i\neq 0)=C(h_i) ,$$

where $C(h_i)$ describes the long-range part of the wall interaction.

The connection with the disjoining pressure formalism is given by the following development. Let us consider a film of liquid B, of thickness h, in equilibrium with a phase A on top of a substrate W. According to [11] we have

$$f=\gamma_{BW}+\gamma_{AB}(\theta=0)+P(h) , \tag{9}$$

where f is the free energy per unit area for the A/W interface, $\gamma_{AB}(\theta=0)$ is the interfacial tension of the flat interface ($\theta=0$), γ_{BW} is the free energy per unit area for contact between the phase B and the wall W, and $P(h)$ is the "free energy" associated to the interaction between the A/B and B/W interfaces. Within our solid-on-solid models, we have

$$f=-\frac{1}{\beta}\lim_{L\to\infty}\frac{1}{L}\ln\left\{\sum_{h_0\in\mathbb{Z}^+}\cdots\sum_{h_L\in\mathbb{Z}^+}e^{-\beta H(h_0\cdots h_L)}\right\} \tag{10}$$

which, by definition of H [Eq. (8)] can be rewritten as

$$f=J_{BW}-\frac{1}{\beta}\lim_{L\to\infty}\frac{1}{L}\ln\left[\sum_{h_0=0,h_1\in\mathbb{Z}}\cdots\sum_{h_{L-1}\in\mathbb{Z},h_L=0}\exp\left[-\beta J_{AB}\sum_i(|h_{i+1}-h_i|+1)\right]\right]$$
$$+\frac{1}{\beta}\lim_{L\to\infty}\frac{1}{L}\ln\left[\sum_{h_0=0,h_1\in\mathbb{Z}}\cdots\sum_{h_{L-1}\in\mathbb{Z},h_L=0}\exp\left[-\beta J_{AB}\sum_i(|h_{i+1}-h_i|+1)\right]\right]$$
$$-\frac{1}{\beta}\lim_{L\to\infty}\frac{1}{L}\ln\left[\sum_{h_0\in\mathbb{Z}^+}\cdots\sum_{h_L\in\mathbb{Z}^+}\exp\left[-\beta J_{AB}\sum_i(|h_{i+1}-h_i|+1)-\beta\sum_i\mu(h_i)\right]\right] .$$

Since we do not take into account the internal structure of the liquid B, we have $J_{BW}=\gamma_{BW}$. This leads to

$$f=\gamma_{BW}+\gamma_{AB}(\theta=0)-\frac{1}{\beta}\lim_{L\to\infty}\frac{1}{L}\ln\frac{\displaystyle\sum_{h_0\in\mathbb{Z}^+}\cdots\sum_{h_L\in\mathbb{Z}^+}\exp\left[-\beta J_{AB}\sum_i(|h_{i+1}-h_i|+1)-\beta\sum_i\mu(h_i)\right]}{\displaystyle\sum_{h_0=0,h_1\in\mathbb{Z}}\cdots\sum_{h_{L-1}\in\mathbb{Z},h_L=0}\exp\left[-\beta J_{AB}\sum_i(|h_{i+1}-h_i|+1)\right]} .$$

This can be written as

$$f=\gamma_{BW}+\gamma_{AB}(\theta=0)-\frac{1}{\beta}\lim_{L\to\infty}\frac{1}{L}\ln\left\langle\prod_i e^{-\beta\mu(h_i)}Y(h_i)\right\rangle , \tag{11}$$

where the average $\langle\ \rangle$ has to be taken with respect to the probability distribution induced by the flat free interface. The function $Y(h_i)$ is a step function which takes the value 1 if its argument is positive and 0 otherwise.

Then, comparing with (9), we find

$$P(h)=-\frac{1}{\beta}\lim_{L\to\infty}\frac{1}{L}\ln\left\langle\prod_i e^{-\beta\mu(h_i)}Y(h_i)\right\rangle . \tag{12}$$

If we consider the complete wetting regime, it is expected that the most probable profile has to be a film of uniform thickness h. Neglecting the fluctuations, we get

$$P(h)=\mu(h) .$$

We also know [11] that

$$P(z)=\int_z^\infty\pi(h)dh , \tag{13}$$

where $\pi(h)$ is the disjoining pressure.

Then we have

$$\pi(h)=-\frac{\partial P(h)}{\partial h}=\frac{1}{\beta}\frac{\partial}{\partial h}\left[\lim_{L\to\infty}\frac{1}{L}\ln\left\langle\prod_i e^{-\beta\mu(h_i)}Y(h_i)\right\rangle\right] . \tag{14}$$

Let us now consider different particular cases.

A. The contact wall potential

The contact wall model may be rewritten as

$$\mu(0)=J_{AW}-J_{BW}-J_{AB} ,$$
$$\mu(1)=\mu(2)=\cdots=0 .$$

For this model, we have performed several numerical experiments using the same procedure. Starting from a given initial drop of fixed volume, we have studied the time evolution of the shape of the drop, i.e., as a function of the number of Monte Carlo steps per site (MCS/site.)

Averages over the profiles corresponding to several experiments lead to an estimate of the profile density of the drop. For instance, we have reproduced in Fig. 2 the density of the profile after different times. For this short-range interaction model, we have observed the ex-

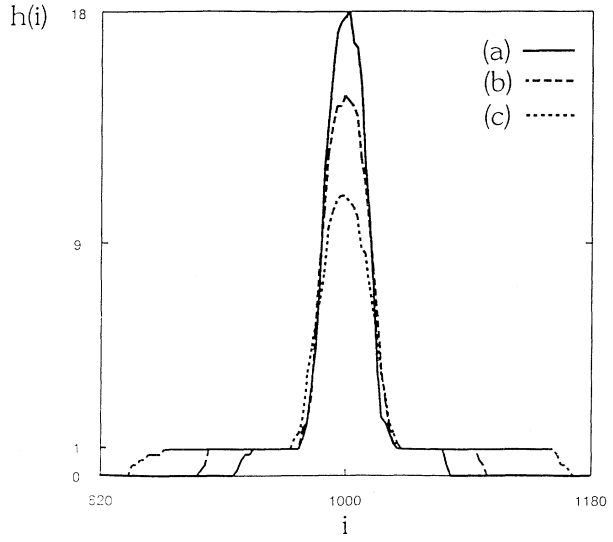

FIG. 2. Time evolution of the averaged profile over five independent experiments of a drop with $\beta J_{AB}=4$ and $\beta(J_{AW}-J_{BW})=7$, after (a) 6×10^6 MCS/site, (b) 13×10^6 MCS/site, and (c) 4×10^7 MCS/site.

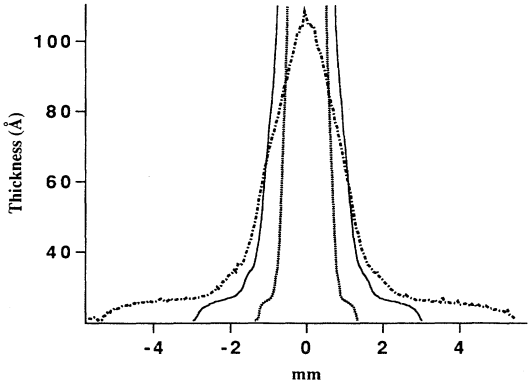

FIG. 4. Ellipsometric thickness profile of a PDMS drop spreading on a cleaned bare wafer. The characteristics of the oil are molecular weight $M_p=9.7$ kg mol^{-1}, viscosity 0.2 Pa s, polydispersity index 1.09, surface tension $\gamma_{AB}=21$ mN m^{-1}. The top of the two first profiles is out of scale. First profile (dotted) 19 h after drop deposition, second profile (full line) 95 h, last profile (dashed) 263 h. The step growing at the bottom of the drop is a 7-Å thick monolayer of molecules in a flat configuration.

istence of a precursor film of one layer thickness. We also observe in this case that the only layer which grows is the first one, the length of which goes linearly with $\sqrt{t}$ as shown in Fig. 3.

The situation represented in Fig. 2 corresponds to the case where the driving term for spreading acts only on the first monolayer. This situation is recovered in experiments when the first monolayer has a very strong interaction with the surface. This is the case for the profile reported in Fig. 4, where the PDMS drop spreads on a bare wafer, cleaned by an oxygen flow under uv illumination, which provides a high-energy surface.

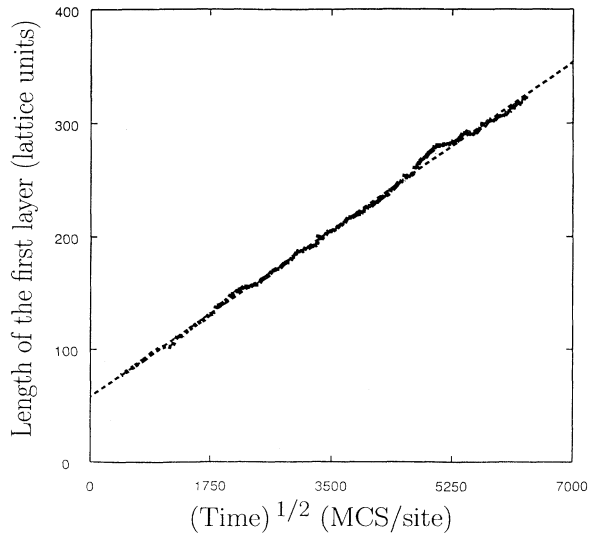

FIG. 3. The time evolution of the length of the first layer for the averaged profile of the SOS drop of Fig. 2.

For different values of the microscopic couplings J_{AB} and J_{AW}, J_{BW}, we have studied the diffusive constants D, where D has been computed by a linear fitting of the radius of the first layer as a function of the square root of the number of MCS/site. Out of these results, it seems that the main parameter is the molecular-molecular interaction typical of the viscosity of the fluid as observed experimentally.

B. More general models

Let us now consider more general models to describe the possible existence of a precursor film of two or three layers thickness.

For that, we modify the Hamiltonian (8) by introducing a new wall interaction of the form

$$\mu(0)=J_{AW}-J_{BW}-J_{AB}\ ,$$
$$\mu(1)=C_1\ ,$$
$$\mu(2)=C_2\ ,$$
$$\vdots$$

where $|C_1|>|C_2|>|C_3|>\cdots$ describe the long-range part of the wall interaction with $\lim_{n\to\infty}C_n=0$ in such a way that $\lim_{h\to\infty}P(h)=0$.

Choosing, for instance, the wall interaction represented in Fig. 5, the configuration which minimizes $\mu(h)$ corresponds to a profile with a precursor film of two layers thickness. In Fig. 6, we observe this formation of a bilayer film which behaves diffusively as a function of the time.

This is in agreement with the experimental observations reproduced in the following section and can be interpreted as a result of a competition between a long-range attraction and a short-range repulsion. It appears

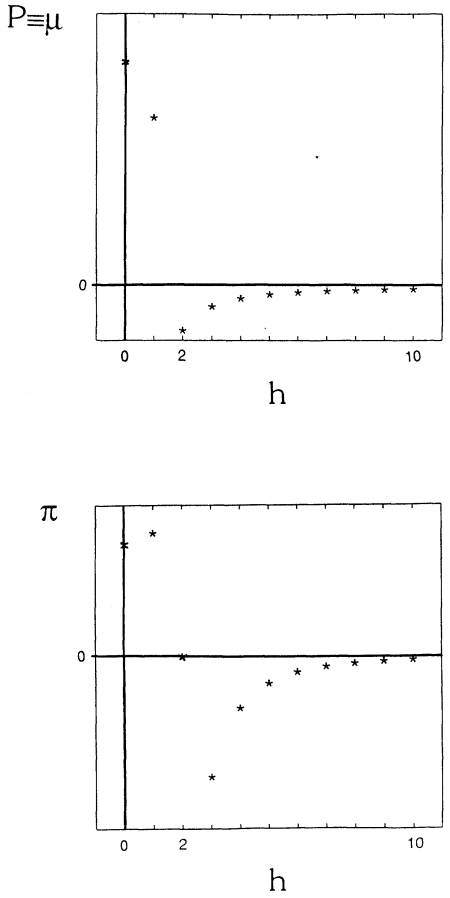

FIG. 5. Wall interaction μ and the corresponding disjoining pressure π as a function of the height.

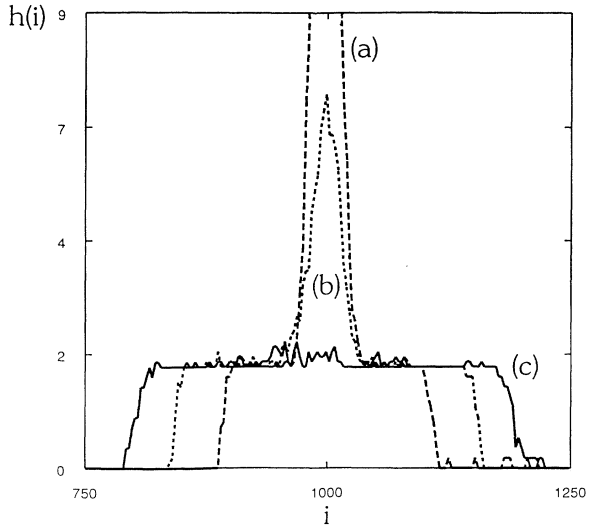

FIG. 6. Time evolution of the profile of a drop with $\beta J_{AB}=2$, $\beta(J_{AW}-J_{BW})=4$ and for the potential of Fig. 5, after (a) 375×10^6 MCS/site, (b) 9×10^6 MCS/site, and (c) 15×10^7 MCS/site for 10 experiments.

that the different simulated profiles are very sensitive to the choice of the wall interaction μ. In particular, we can also recover a step-pyramidal shape which is in agreement with the experimental observations.

IV. EXPERIMENTAL OBSERVATIONS

To investigate the vicinity of the wetting transition, we have used two types of grafted layers, and on each substrate a series of oils with different molecular weights. As a matter of fact, the surface tension of PDMS increases with the chain length of the polymer, at least for the short chains. This allows us to cross the transition where $\gamma_{AW}-\gamma_{BW}=\gamma_{AB}$, by combining changes in the surface $(\gamma_{AW}-\gamma_{BW})$ and in the oil (γ_{AB}). It is customary to introduce here the common value of $(\gamma_{AW}-\gamma_{BW})$ and γ_{AB} at the transition, that is the critical surface tension γ_c of the surface for the series of liquids investigated (here, the various PDMS), which does not depend on the particular oil in the series. If $\gamma_{AB}<\gamma_c$, the oil wets, if $\gamma_{AB}>\gamma_c$, it does not.

The PDMS we use have molecular weights in the range 2 to 16 kg mol^{-1}, and surface tensions in the range 20.6 to 21.1 mN m^{-1}. The critical surface tension of the substrates has to be in this range, if we want to cross the transition by varying the chain length of the PDMS. This can be achieved in the following two ways [10]:

(i) By grafting on the surface alkyl chains terminated by methyl ends. For long enough chains, typically 12 or 16 carbons, critical surface tensions around 20.6 mN m^{-1} are obtained. We prepared such surfaces, according to the procedure described by Brzoska [12].

(ii) By absorbing on the surface a layer of PDMS with a given molecular weight. The critical surface tension of

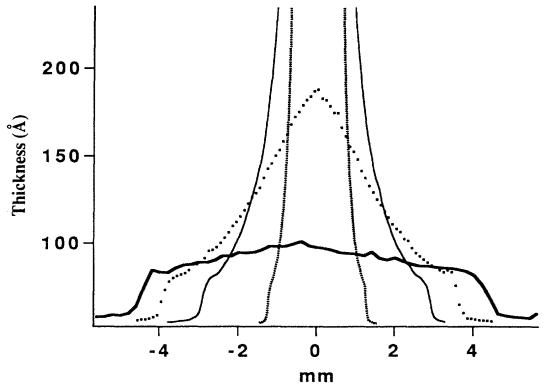

FIG. 7. Ellipsometric thickness profile of a PDMS drop spreading on a wafer bearing a grafted layer of methyl-terminated alkyl chains with 16 carbons. The characteristics of the oil are: molecular weight $M_p=2$ kg mol^{-1}, viscosity 0.02 Pa s, polydispersity index 1.6, surface tension $\gamma_{AB}=20.6$ mN m^{-1}. The top of the two first profiles is out of scale. First profile (dotted) 2.5 h after drop deposition, second profile (full light line) 20 h, third profile (dots) 44.5 h, last profile (full heavy line) 93.3 h. The thickness of the step at the bottom of the drop is 23 Å (approximately three times the molecule size).

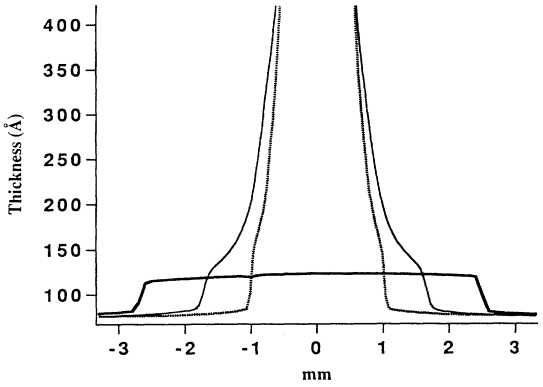

FIG. 8. Ellipsometric thickness profile of a PDMS drop spreading on a wafer bearing an anchored layer of hydroxyl-terminated PDMS. The thickness of the absorbed layer is 70 Å, the molecular weight of this oil is 8 kg mol^{-1} (viscosity 0.18 Pa s, polydispersity index 1.14, surface tension 20.9 mN m^{-1}). The characteristics of the oil in the drop are: molecular weight 6.7 kg mol^{-1}, (viscosity 0.12 Pa s, polydispersity index 1.06, surface tension $\gamma_{AB}=20.9$ mN m^{-1}). The top of the two first profiles is out of scale. First profile (dotted) 16 h after drop deposition, second profile (full light line) 46 h, last profile (full heavy line) 281 h. The thickness of the step at the bottom of the drop is 42 Å (approximately six times the molecule size).

the substrate is close to the surface tension of the grafted PDMS: lighter oils will wet, because their surface tension is lower than the one of the absorbed layer, the heavier will not. In practice, we use hydroxyl-terminated PDMS (PDMS-OH), because of the strong anchoring of the hydroxyl ends on the clean wafers, allowing to obtain well defined layers [13].

Figures 7 and 8 provide examples of drop shapes close to the wetting transition: the microscopic model accounts satisfactory for the thick first step at the bottom of the drop, the thickness of which diverges at the transition. Moreover, interaction parameters can easily be adjusted to mimic any particular drop shape. This model is potentially more quantitative than the ones using approximate formulae for the long-range part of the disjoining pressure [10].

ACKNOWLEDGMENTS

The authors acknowledge financial support from the Tournesol program which makes this collaboration possible. This text also presents research results of the Belgian program on Interuniversity Poles of Attraction initiated by the Belgian State, Prime Minister's Office, Science Policy Programming.

APPENDIX: THE VALIDITY OF THE DYNAMICS

To check the consistency of the dynamics, we focus on the partial wetting regime given by $\gamma_{AW}-\gamma_{BW}<\gamma_{AB}(\theta=0)$. Indeed, for these conditions, we must recover, at equilibrium, a drop of a certain shape on top of the substrate. This shape is exactly computable from the interfacial tension associated to the model. This tension is angular dependent due to the lattice approximation and can be computed as

$$\gamma(\theta,\beta)=-\frac{1}{\beta}\lim_{N\to\infty}\frac{\cos\theta}{N}\ln\Xi(N,\theta,\beta)\ , \tag{15}$$

where $\Xi(N,\theta,\beta)$ is the partition function corresponding to an interface with an angle θ with respect to the horizontal plane.

The corresponding equilibrium shape is given by the Wulff construction modified by the interactions with the wall. For completeness, let us here present the result. The equilibrium shape of a drop, up to a dilatation, is given by the Legendre transform of the interfacial tension as a function of $\tan\theta$ [14].

The Laplace transform of $\Xi(N,\theta,\beta)$ is defined by

$$\Theta(N,x,\beta)=\sum_{N\tan\theta\in\mathbb{Z}}e^{-\beta Nx\tan\theta}\Xi(N,\theta,\beta)\ , \tag{16}$$

where the condition of a fixed slope is replaced by an "external field" associated to the x coordinate.

Then the corresponding Legendre transform of $\gamma(\theta,\beta)$ is given by the y coordinate

$$y=-\frac{1}{\beta}\lim_{N\to\infty}\frac{1}{N}\ln\Theta(N,x,\beta)\ . \tag{17}$$

For the considered model defined in Eq. (1), this function can be easily computed and the result is given by

$$y=J_{AB}-\frac{1}{\beta}\ln\frac{\sinh\beta J_{AB}}{\cosh\beta J_{AB}-\cosh\beta x}\ . \tag{18}$$

To obtain the shape of the droplet, up to a dilatation, we draw the crystal shape given by (18) and fix the wall at height $\gamma_{AW}-\gamma_{BW}$ from the plane of symmetry of the crystal shape.

To compute the wall free energy $\gamma_{AW}-\gamma_{BW}$, we use the results of [15].

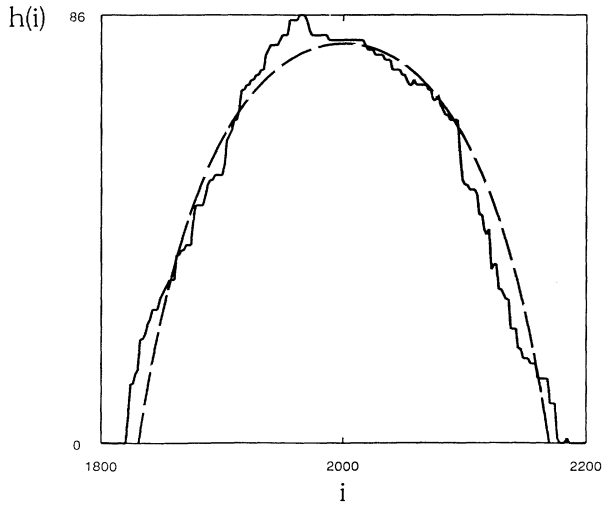

FIG. 9. Equilibrium profile for partial wetting of a triangular drop which volume = 20 000 [$\beta J_{AB}=2$, $\beta(J_{AW}-J_{BW})=1$]. The dashed line represents the corresponding Wulff shape.

$$\gamma_{AW} = -\frac{1}{\beta}\ln\lambda_{\max} , \tag{19}$$

where $\lambda_{\max}$ is the largest λ solution of the following two equations:

$$w + \frac{1}{w} = 2(\cosh J_{AB} - \frac{1}{\lambda}\sinh J_{AB}) ,$$

$$e^{-(J_{AW}-J_{BW}-J_{AB})} - \lambda + e^{-J_{AB}} \frac{w}{1-e^{-J_{AB}}w} = 0 ,$$

with a contact wall potential given by

$$H(\{h_i\}) = J_{AB} \sum_{i=0}^{L-1} |h_{i+1} - h_i| + (J_{AW} - J_{BW} - J_{AB}) \sum_{i=0}^{L} \delta_{h_i,0} . \tag{20}$$

If we consider the Hamiltonian (1) we have here

$$\gamma_{AW} = -\frac{1}{\beta} \lim_{L\to\infty} \frac{1}{L} \ln Z_L , \tag{21}$$

where

$$Z_L = \sum_{h_0 \in \mathbb{Z}^+} \cdots \sum_{h_L \in \mathbb{Z}^+} e^{-\beta H(h_0, \ldots, h_L)}$$

with $H(h_0, \ldots, h_L)$ defined in (1). This leads to

$$\gamma_{AW} = (J_{AB} + J_{BW}) - \frac{1}{\beta} \lim_{L\to\infty} \frac{1}{L} \ln \left[\sum_{h_0 \in \mathbb{Z}^+} \cdots \sum_{h_L \in \mathbb{Z}^+} e^{-\beta H(\{h_i\})} \right] , \tag{22}$$

where $H(\{h_i\})$ has been defined in (20).

$$\gamma_{AW} = J_{AB} + J_{BW} - \frac{1}{\beta}\ln\lambda_{\max} . \tag{23}$$

The wall free energy γ_{BW} being equal to the constant J_{BW}, we then have

$$\gamma_{AW} - \gamma_{BW} = J_{AB} - \frac{1}{\beta}\ln\lambda_{\max} \tag{24}$$

with (18) and (24), we can draw the equilibrium shape of a drop on the top of a wall in the partial wetting regime.

We have considered an initial triangular drop ($V = 20\,000$) which we let evolve as a function of the number of Monte Carlo steps per site to the Wulff shape. Figure 9 represents the final profile after 100×10^6 MCS/site. As can be easily seen, the agreement between the simulated profile and the computed one (dashed line in the figure) is quite satisfactory.

[1] F. Heslot, A. M. Cazabat, and P. Levinson, Phys. Rev. Lett. **62**, 1286 (1989).

[2] F. Heslot, A. M. Cazabat, P. Levinson, and N. Fraysse, Phys. Rev. Lett. **65**, 599 (1990).

[3] J. De Coninck, N. Fraysse, M. P. Valignat, and A. M. Cazabat, Langmuir **9**, 1906 (1993).

[4] F. Heslot, N. Fraysse, and A. M. Cazabat, Nature **338**, 640 (1989).

[5] J. Yang, J. Koplik, and J. R. Banavar, Phys. Rev. Lett. **67**, 3539 (1991).

[6] J. A. Nieminen, D. B. Abraham, M. Karttunen, and K. Kaski, Phys. Rev. Lett. **69**, 124 (1992).

[7] D. Abraham, P. Collet, J. De Coninck, and F. Dunlop, Phys. Rev. Lett. **65**, 195 (1990).

[8] J. De Coninck, F. Dunlop, and F. Menu, Phys. Rev. E **47**, 1820 (1993).

[9] N. Fraysse, M. P. Valignat, A. M. Cazabat, F. Heslot, and P. Levinson, J. Colloid Interface Sci. **158**, 27 (1993).

[10] M. P. Valignat, N. Fraysse and A. M. Cazabat, Langmuir (to be published).

[11] P. G. de Gennes, Rev. Mod. Phys. **57**, 827 (1985).

[12] J. B. Brzoska, Thesis, University Paris VI, 1993; J. B. Brzoska, N. Shahidzadeh and F. Rondelez, Nature (to be published).

[13] M. P. Valignat, N. Fraysse, A. M. Cazabat, and F. Heslot, Langmuir, **9**, 601 (1993).

[14] J. De Coninck, R. Kotecky, L. Laanait, and J. Ruiz, Physica A **189**, 616 (1992).

[15] J. M. J. van Leeuwen and H. J. Hilhorst, Physica A **107**, 319 (1981).